Final Technical Report

1 JUL 96 to 31 JUL 99

Proposal Title: "Deformation and Fracture of
Laminated Intermetallic Materials"

Grant Number: F49620-96-1-0238

Principal Investigators: P.M. Anderson and H.L. Fraser

Department of Materials Science and Engineering
Ohio State University
2041 College Road
Columbus, OH 43210-1179

20000324 044

0 2 MAR 2000 NA/*

REPORT DOCUMENTATION PAGE

AFRL-SR-BL-TR-00-

00 77

The public reporting burden for this collection of information is estimated to average 1 hour per response,
gathering and maintaining the data needed, and completing and reviewing the collection of information. Send
of information, including suggestions for reducing the burden, to Department of Defense, Washington
[0704-0188), 1215 Jefferson Davis Highway, Suite 1204, Arlington, VA 22202-4302. Respondents should
subject to any penalty for failing to comply with a collection of information if it does not display a currently va
PLEASE DO NOT RETURN YOUR FORM TO THE ABOVE ADDRESS.

1. REPORT DATE *(DD-MM-YYYY)*	2. REPORT TYPE	3. DATES COVERED *(From - To)*
29-FEB-00	FINAL	1 JUL 96 to 31 JUL 99

4. TITLE AND SUBTITLE	5a. CONTRACT NUMBER
Deformation and Fracture of Laminated Intermetallic Materials	F49620-96-1-0238

5b. GRANT NUMBER

5c. PROGRAM ELEMENT NUMBER

6. AUTHOR(S)	5d. PROJECT NUMBER
ANDERSON, PETER, M. FRASER, HAMISH, L.	

5e. TASK NUMBER

5f. WORK UNIT NUMBER

7. PERFORMING ORGANIZATION NAME(S) AND ADDRESS(ES)	8. PERFORMING ORGANIZATION REPORT NUMBER
THE OHIO STATE UNIVERSITY RESEARCH FOUNDATION 1960 KENNY ROAD, COLUMBUS, OH 43210	

9. SPONSORING/MONITORING AGENCY NAME(S) AND ADDRESS(ES)	10. SPONSOR/MONITOR'S ACRONYM(S)
AFOSR/PKC 801 N. RANDOLPH STREET ARLINGTON, VA 22203	11. SPONSOR/MONITOR'S REPORT NUMBER(S)

12. DISTRIBUTION/AVAILABILITY STATEMENT

NO RESTRICTIONS

DISTRIBUTION STATEMENT A
Approved for Public Release
Distribution Unlimited

13. SUPPLEMENTARY NOTES

14. ABSTRACT
This project began with both an experimental effort to produce γ-Ni(Al)/γ'-Ni3Al multila
and a modeling effort to understand the strength of such multilayers. The experimental work
progressed to the point that, for the first time known to the investigators, γ-Ni(Al)/γ'-Ni3Al
multilayers have been produced by magnetron sputtering. Samples with individual layer thickne
ranging from 20nm 20nm to 120nm 120nm have been produced and two epitaxies, <001> and <111>,
been achieved. With respect to modeling, results (see **Fig. 28**) show how the choice of layer
thickness, volume fraction, and interfacial strength affect the strength of such materials.
Peierls model of resistance of interfaces to slip transmission also was developed in an effort
understand the principal role of atomic bonding properties and modulus mismatch across interfa
the strength of interfaces to transmission.

15. SUBJECT TERMS

Multilayers, Nanolaminated composites, Strength, Magnetron sputtering, Fracture, Dislocation transmission, Interfacial strength.

16. SECURITY CLASSIFICATION OF:			17. LIMITATION OF ABSTRACT	18. NUMBER OF PAGES	19a. NAME OF RESPONSIBLE PERSON
a. REPORT	b. ABSTRACT	c. THIS PAGE	UU	37	Anderson, Peter, M.
					19b. TELEPHONE NUMBER *(include area code)* 614-292-0176

Standard Form 298 (Rev. 8/98)
Prescribed by ANSI Std. Z39.18

1. **Identification Material**
   P.I. Names: P.M. Anderson and H.L. Fraser
   Proposal Title: "Deformation and Fracture of Laminated Intermetallic
                     Materials"
   Institution: Ohio State University Research Foundation
                     Grants and Contracts Management
                     1960 Kenny Road
                     Columbus, OH 43210-1063
   Contract Number: F49620-96-1-0238

2. **Objective** (as stated in the original proposal)
   The purpose of the proposed work was to develop an understanding of the
   influence of scale and the nature of interfaces on the deformation and
   fracture behavior of multilayered metallic/intermetallic materials.

3. **Status of the effort**
   This project began with both an experimental effort to produce γ-
   Ni(Al)/γ'-Ni$_3$Al multilayers and a modeling effort to understand the
   strength of such multilayers. The experimental work progressed to the
   point that, for the first time known to the investigators, γ-Ni(Al)/γ'-
   Ni$_3$Al multilayers have been produced by magnetron sputtering. Samples
   with individual layer thicknesses ranging from 20nm/20nm to 120nm/120nm
   have been produced and two epitaxies, <001> and <111>, have been
   achieved.

   With respect to modeling, we have predicted modes of plastic
   deformation that occur in such multilayered materials. The results (see
   Fig. 28) show how the choice of layer thickness, volume fraction, and
   interfacial strength affect the strength of such materials. A Peierls
   model of resistance of interfaces to slip transmission also was developed
   in an effort to understand the principal role of atomic bonding
   properties and modulus mismatch across interfaces, on the strength of
   interfaces to transmission.

   In summary, the effort successfully produced Ni(Al)/γ'-Ni$_3$Al
   multilayers, a preliminary study of the fracture characteristics of such
   multilayers was conducted, and corresponding models of plasticity have
   been made to capture the strength of such materials, as a function of
   layer thickness and epitaxy.

   Particular accomplishments and new findings are discussed in the
   following section.

4. **Accomplishments/New Findings**
   a. <u>Processing of γ-Ni(Al)/γ-Ni$_3$Al multilayered thin films</u>

      Multilayered γ-Ni(Al)/γ'-Ni$_3$Al thin films with various
      individual layer thickness (typically 120nm/120nm, and
      20nm/20nm) and overall thickness of approximately 6-8 μm
      were produced by physical vapor deposition under ultra high
      vacuum conditions, using a solid solution Ni-10wt%Al target
      and an ordered intermetallic Ni$_3$Al target.
      Multilayers with <001> epitaxy were produced by pre-baking
      <001> cleaved NaCl substrates at approximately 450C for 30

minutes in order to alleviate any moisture absorbed on the surface. During deposition, the substrate temperature was maintained at approximately 500C. No heating was necessary to produce the <111> epitaxy. A stainless steel mask was used to produce dogbone-shaped samples designed for subsequent tensile testing. After deposition, samples were removed by dipping the surface of the substrate into water and allowing the multilayer to float off. Hence, all multilayer samples were "free-standing". Scanning electron micrographs of some polished γ-Ni(Al)/γ'-Ni$_3$Al multilayered thin films are shown in **Figs. 1 to 3**.
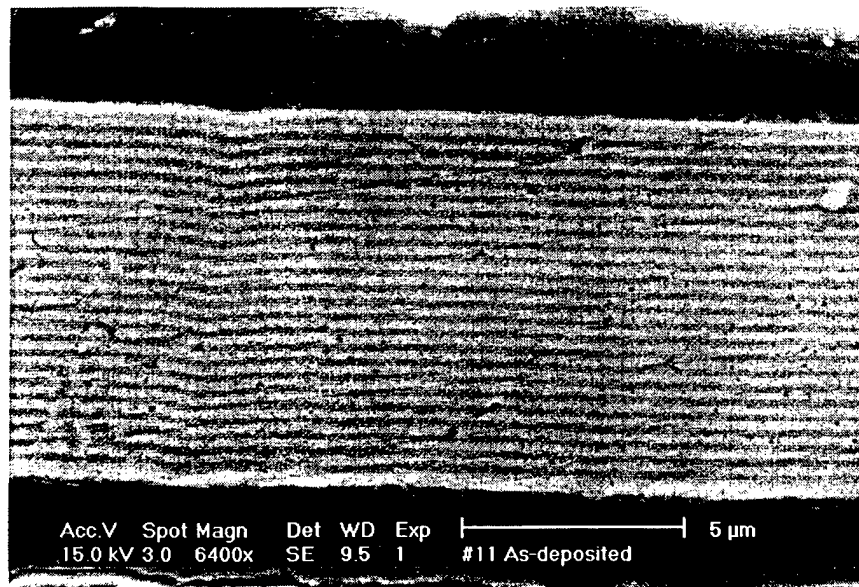
Fig. 1:   SEM micrograph of polished <001> 120nm/120nm multilayered γ-Ni(Al)/γ'-Ni$_3$Al sample (#11-1).
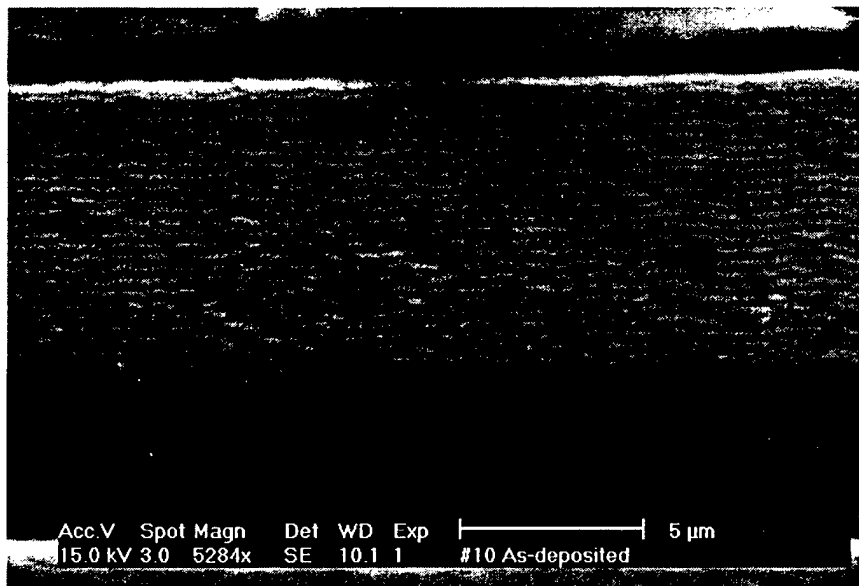
Fig. 2:   SEM micrograph of a polished <111> 120nm/120nm multilayered γ-Ni(Al)/γ'-Ni$_3$Al sample (#10-1).
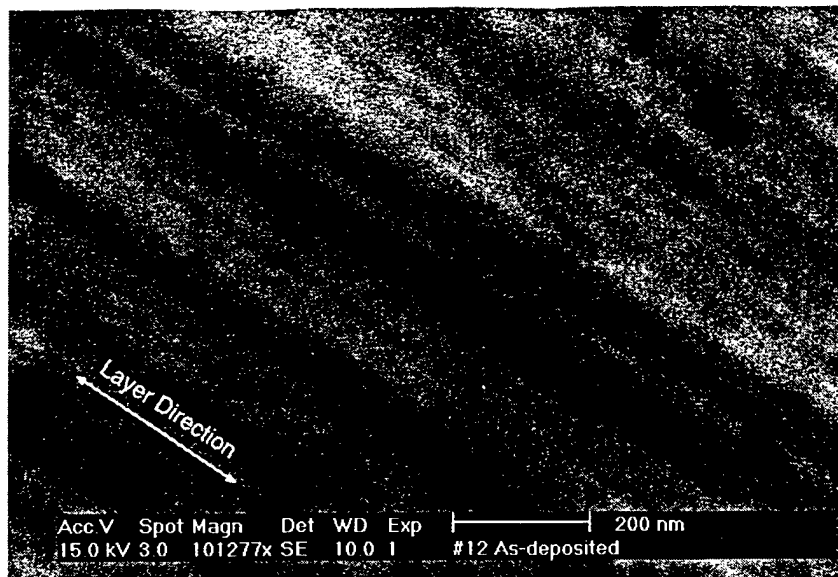
Fig. 3:   SEM micrograph of polished <111> 20nm/20nm multilayered
           γ-Ni(Al)/γ'-Ni$_3$Al sample (#12-1).

Ni/Ni$_3$Al multilayers were also fabricated in the custom-built UHV
magnetron sputtering unit during year 2 of the investigation. A
detailed description of the sputtering unit is given in [4]. In order
to sputter Ni, which is a ferromagnetic material, the permanent
magnets in the magnetron gun were replaced with stronger magnets with
field strengths ~ 0.5 tesla. Additionally, a new load-lock arrangement
was added to the system which permits loading and removal of
substrates into the system without exposing the main chamber to
atmospheric pressure. This allows for deposition of a larger number of
films in a shorter time period.

One of the important achievements in the processing of Ni/Ni$_3$Al
multilayers was to determine the influence of substrate materials and
conditions on the epitaxy and growth morphology of these multilayers.
Initially, depositions were carried out on oxidised Si (100)
substrates which had a 200 nm thick amorphous oxide layer on the
surface. Three different substrate temperatures were studied: room
temperature, 200 C and 400 C. A well-defined multilayer morphology
was observed for the films deposited at room temperature and 200 C.
In both cases, the microstructure consists of columnar grains with a
strong <111> epitaxy. Interestingly, a significantly large amount of
intermixing between the Ni and Ni$_3$Al layers occurred for the film
deposited at 400 C, leading to a breakdown of the multilayer
morphology.

The next phase of experiments concentrated on epitaxial growth of
<100> Ni/Ni$_3$Al multilayers which would result in an orientation
relationship between the Ni and Ni$_3$Al similar to that observed in
superalloys. Films were deposited on single crystal Cu (100)
substrates with the objective of forcing the <100> epitaxy from the Cu
to the growing film. Initially a thick buffer layer of pure Ni was
grown at 600 C followed by the deposition of the multilayer at 200 C.
Subsequent x-ray analysis showed that the multilayer had grown with

the <111> epitaxy and not <100> epitaxy. Subsequently, single crystal (100) NaCl substrates have been used. Films grown at room temperature and also at 350 C on NaCl substrates exhibited a <111> epitaxy.

A significant observation is that films grown on the same substrate at temperatures in excess of 400 C exhibit a strong <100> epitaxy. Therefore, it is possible to grow <100> Ni/Ni$_3$Al multilayers on (100) NaCl substrates at high deposition temperatures. An added advantage of using NaCl is that the substrate can be dissolved post deposition to give free standing films. Tom Moffat (NIST) is acknowledged for collaboration on substrate preparation and Tim Foecke (NIST) for providing the copper substrates.

b. <u>Microstructural characterization of Ni/Ni$_3$Al multilayered thin films</u>

Based on the discussion in the previous section, it is evident that the two epitaxies observed in Ni/Ni$_3$Al multilayers were <111> and <100>. In this section a detailed discussion of the microstructural features observed in these two different epitaxies is presented. For the <111> epitaxy, the multilayer specimen studied consisted of 37 bilayers with a bilayer thickness ~ 260 nm deposited on a single crystal Cu (100) substrate with a sputter deposited Ni buffer layer on the top. The deposition temperature for the multilayer was ~ 200 C. **Figure 4** shows a x-ray diffraction pattern from this multilayer. The large intensity of the <111> peaks of Ni and Ni$_3$Al suggests the strong <111> epitaxy in this multilayer.

A cross-section bright filed TEM micrograph from this multilayer is shown in **Figure 5**. The multilayered morphology is evident in this image. The layers with the darker contrast correspond to the Ni phase and those with the lighter contrast correspond to the Ni$_3$Al phase. Since Ni and Ni$_3$Al do not have a large difference in mean atomic masses, the difference in electron scattering factors between these two phases is not expected to be very large resulting in relatively low contrast differences between the two phases for the same thickness.
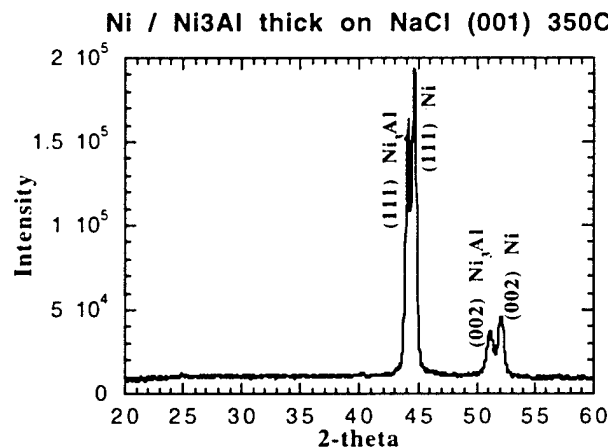

Figure 4: X-ray diffraction pattern for a Ni/Ni$_3$Al multilayer with <111> epitaxy.
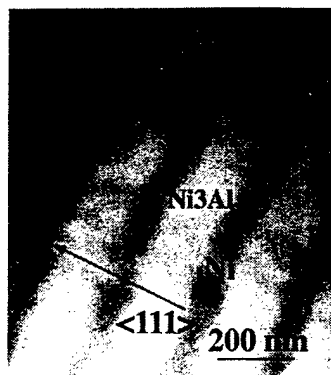
Figure 5:
Corresponding
TEM micrograph
for the Ni/Ni₃Al
multilayer with
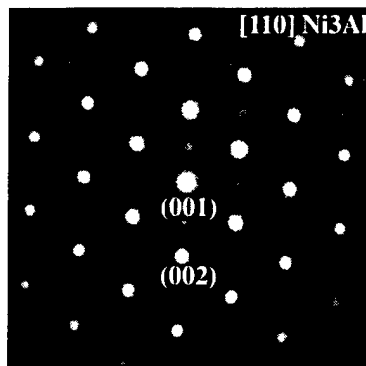<111> epitaxy.

Figure 6:
Corresponding
<110> zone axis
microdiffractio
n pattern for
the Ni/Ni₃Al
multilayer with
<111> epitaxy.

The <110> zone axis microdiffraction pattern from the Ni₃Al phase is shown in **Figure 6**. The presence of (100) superlattice reflections in the diffraction pattern suggests that the Ni₃Al phase is ordered and has the $L1_2$ structure in this multilayer. A columnar growth morphology was observed in this multilayer with a significant density of faults in the columnar grains. **Figure 7** shows a typical columnar grain in this multilayer viewed in the cross-section geometry with a large density of faults in the grain. These faults are most likely

Figure 7: Typical
columnar grain
morphology observed
in the Ni/Ni3Al
multilayer with <111>
epitaxy.

twins and stacking faults aligned parallel to the Ni/Ni₃Al interface suggesting that the faults lie parallel to the (111) planes of Ni and

Ni_3Al.

For the <100> epitaxy, a Ni/Ni_3Al multilayer with a bilayer thickness ~ 180 nm was studied. This multilayer was deposited on a single crystal NaCl (100) substrate at a deposition temperature ~ 420 C. The strong <100> epitaxy in this multilayer is evident from the large intensity of the (200) Ni and Ni_3Al peaks in the x-ray diffraction pattern shown in **Figure 8**. Interestingly, the (100)
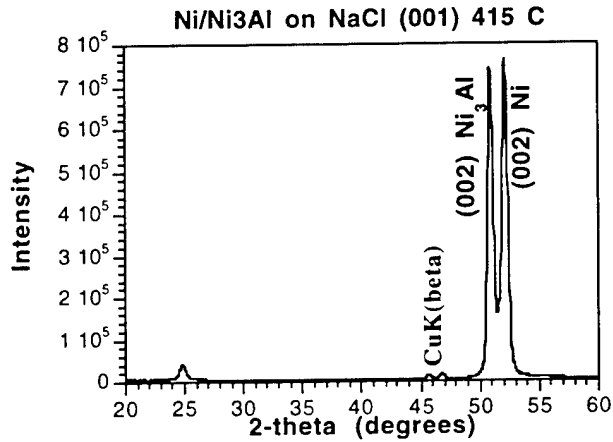

Figure 8: X-ray diffraction pattern for a Ni/Ni3Al multilayer with <100> epitaxy.

superlattice intensity from the Ni_3Al is also seen in this diffraction pattern, suggesting the presence of an $L1_2$ ordered Ni_3Al phase.

Figure 9 is a bright field cross-section TEM micrograph from the multilayer. The difference in contrast between the two phases is low as evident from the image. Faults can be seen in this multilayer too. However, unlike the multilayers with <111> epitaxy, these multilayers have faults that are aligned at an angle to the Ni/Ni_3Al interface. **Figures 10** and **11** are [100] zone axis diffraction patterns from Ni and Ni_3Al respectively.
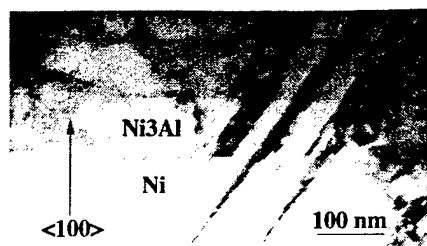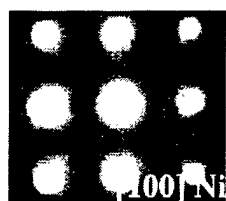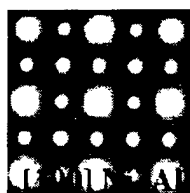
Figure 9:
Corresponding
bright field
cross-section
TEM micrograph
for the Ni/Ni$_3$Al
multilayer with
<100> epitaxy.

(c)   (d)

Figures 10, 11:
Corresponding
zone axis
diffraction
patterns for
the Ni (Fig.
10) and Ni$_3$Al
(Fig. 11)
phases of the
multilayer with
<100> epitaxy.

Figure 12 is a dark field image from this multilayer constructed
using the (100) superlattice reflection from the Ni$_3$Al phase. Due to
the lack of good contrast between the Ni and Ni$_3$Al layers in these
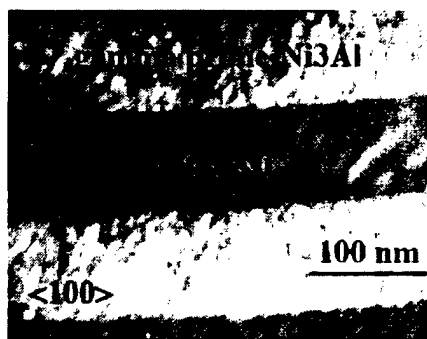multilayers, dark field microscopy is a very useful technique which

Figure 12:
Corresponding
dark field
image using the
(100)
superlattice
reflection from
the Ni$_3$Al phase
of a multilayer
with <100>
epitaxy.

can be exploited to accentuate the contrast between the two layers by
making one of them diffract more strongly than the other.

c. Mechanical behavior of γ-Ni(Al)/γ'-Ni$_3$Al multilayered thin films

Mechanical testing of free standing, ~7µm-thick multilayered samples proved to be difficult. Our testing in a horizontal, table-top, MTS frame revealed that wrinkling of the sample is sensitively dependent on gripping and alignment of the dogbone-shaped samples. The wrinkling produces departures from homogeneous loading and reliable stress-strain behavior is difficult to obtain. Typically, samples failed at varying values of nominal stress, depending on the degree of local stress concentration produced by wrinkling. Our samples have been sent to Prof. William Gerberich for nanoindentation testing, as an alternate mode of mechanical evaluation. Those tests follow the formal end of the project period, but are being conducted to complete results.

d. Tensile fracture behavior of γ-Ni(Al)/γ'-Ni$_3$Al multilayered thin films

Dogbone-shaped samples were loaded in tension until failure and the corresponding fracture surfaces for <001> 120nm/120nm, <001> 20nm/20nm, <111> 120nm/120nm, and <111> 20nm/20nm samples are shown in **Figs. 13 to 16**, respectively.

Two overall trends are observed. First, the <001> epitaxy samples display more ductile fracture surface features than <111> epitaxy samples. Second, the finer, 20nm/20nm, samples exhibit more ductile fracture surface features than the coarser samples of the same epitaxy. Thus, the <001> 20nm/20nm case displays the most ductile fracture surface features while the <111> 120nm/120nm case displays the most brittle fracture surface features.

Comparison of the extreme <001> 20nm/20nm (**Fig. 14**) and <111> 120nm/120nm (**Fig. 15**) cases reveals the range of possible fracture processes in these nanolaminates. The fracture surface of the <001> 20nm/20nm sample is virtually indistinguishable from that of a monolithic sample that has failed by ductile coalescence of cavities. The dimension of the largest cavities in this case spans multiple layer thicknesses, indicating that pronounced codeformation of the Ni and Ni$_3$Al phases occurred. The codeformation is extensive enough so that individual layers can not be discerned. For comparison, the <111> 120nm/120nm sample (**Fig. 15**) is so much more brittle that the layered morphology is revealed by light horizontal markings on the fracture surface. The distance between successive markings corresponds to a bilayer repeat distance. The markings appear to be ridges left by ductile necking down of the Ni layers.

Models of crack advance in the arrester or divider mode predict such ductile ligaments to occur, provided that the more brittle Ni$_3$Al layers crack on both sides of a Ni layer, so that the Ni layer is left as a ductile bridging ligament. A schematic of such a process for the arrester mode of crack propagation is shown in **Fig. 17**. A comparable model for the crack divider orientation involves a non-straight, "fingered" type of crack front which is more advanced in the Ni$_3$Al layers. The Ni layers in between these cracked fingers serve as ductile ligaments in the fracture process zone.
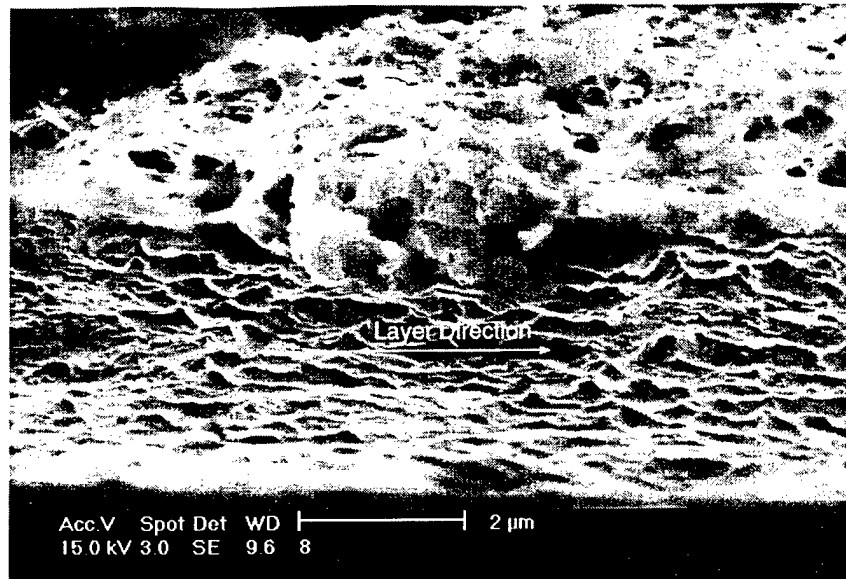
Fig. 13: SEM micrograph of the tensile fracture surface of a <001> 120nm/120nm Ni/Ni$_3$Al multilayered sample (#4-2).
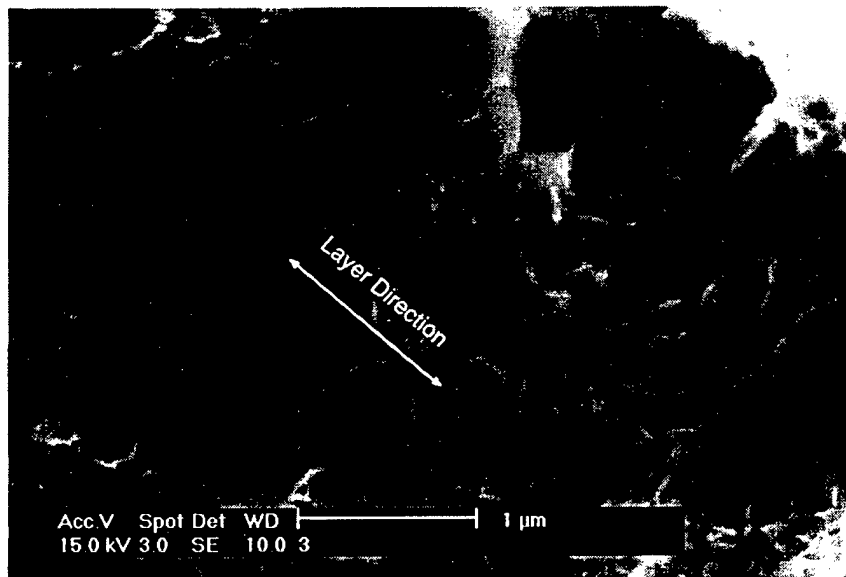

Fig. 14: SEM micrograph of the tensile fracture surface of a <001> 20nm/20nm Ni/Ni$_3$Al multilayered sample (#3-2).

Fig. 15:   SEM micrograph of the tensile fracture surface of a
            <111> 120nm/120nm Ni/Ni$_3$Al multilayered sample (#8-1).

Fig. 16:   SEM micrograph of the tensile fracture surface of a
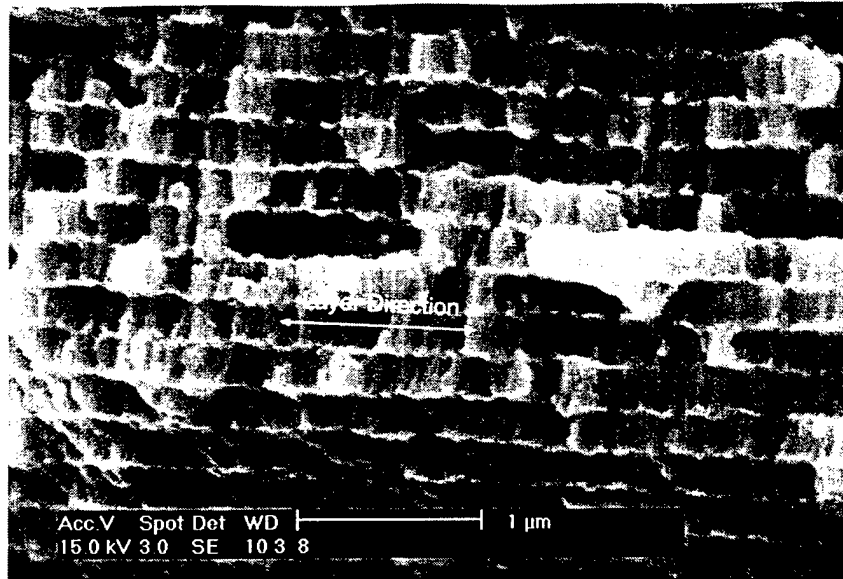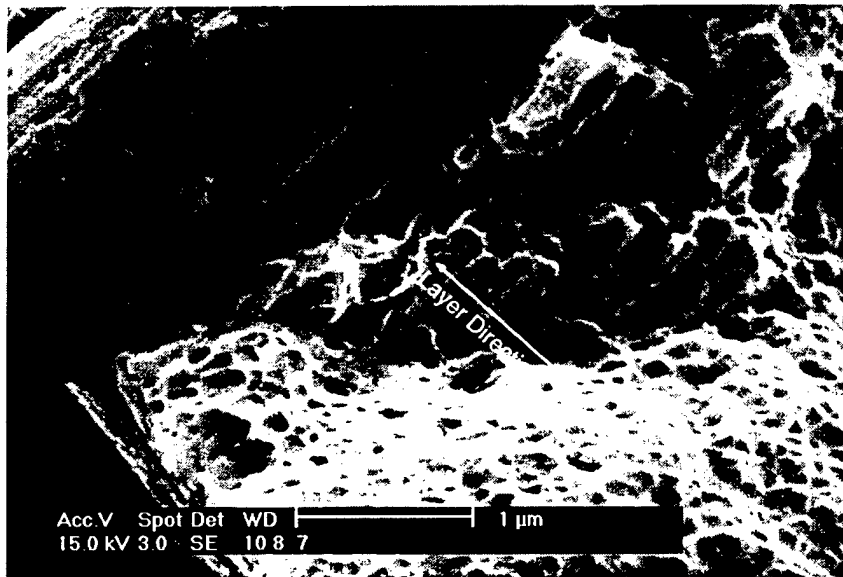   <111> 20nm/20nm Ni/Ni$_3$Al multilayered sample (#7-6).

The <111> 20nm/20nm fractograph (**Fig. 16**) reveals a more brittle, but mixed situation in which ductile void coalescence occurs in some regions (lower right) and more brittle fracture occurs around columnar features (upper left). Between these regions (center), very fine, parallel, white ridges can be discerned. Those striations correspond to the layered structure and, like the 120nm/120nm case, they appear to be caused by ductile ligament formation. Such features suggest that, overall, the <111> epitaxy cases have more brittle fracture surface features than the <001> cases.

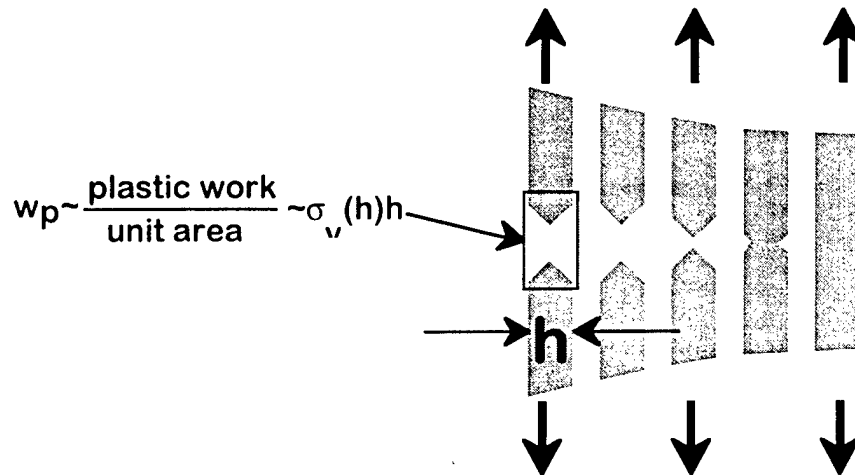$$w_p \sim \frac{\text{plastic work}}{\text{unit area}} \sim \sigma_v(h)h$$

Fig. 17:   Schematic of ductile ligament toughening in a crack arrester mode, in which brittle (Ni_3Al) layers crack first and leave ductile (Ni) layers as bridging ligaments. The ligaments produce parallel ridges on the fracture surface with spacing equal to a bilayer repeat distance.

Figures 18 to 21 show SEM micrographs of the polished *sides* of the fractured, tensile samples, in an effort to determine the more macroscopic nature of the fracture. The <001> 120nm/120nm case (**Fig. 18**) is the most macroscopically ductile sample, since it exhibits significant necking down prior to final failure by shearing across layers. The finer layered <001> 20nm/20nm (**Fig. 19**) and <111> 20nm/20nm (**Fig. 21**) samples fail by local shear at an inclined angle to the tensile direction, with insignificant reduction in cross sectional area. The <111> 120nm/120nm case (**Fig. 20**) displays the most brittle behavior, with tensile failure occurring on a plane approximately perpendicular to the tensile axis and with insignificant reduction in cross sectional area.

To conclude, all failures are classified as macroscopically brittle, in that most of the gage section was undeformed following the test. The <001> 120nm/120nm sample (**Fig. 18**) was the only one tested that displayed any significant reduction in area, and that reduction was limited to just near the fracture surface. Locally, on the fracture surface, the <001> epitaxy samples displayed large amounts of codeformation. The <111> epitaxy samples displayed limited codeformation, so that a distinct layered structure could still be

12/12

observed, even in portions of the 20nm/20nm fracture surface. The fracture surfaces of <111> epitaxy samples are consistent with a fracture process in which the more brittle, Ni$_3$Al, layers may have cracked first, so that Ni layers are left as ductile bridging ligaments.
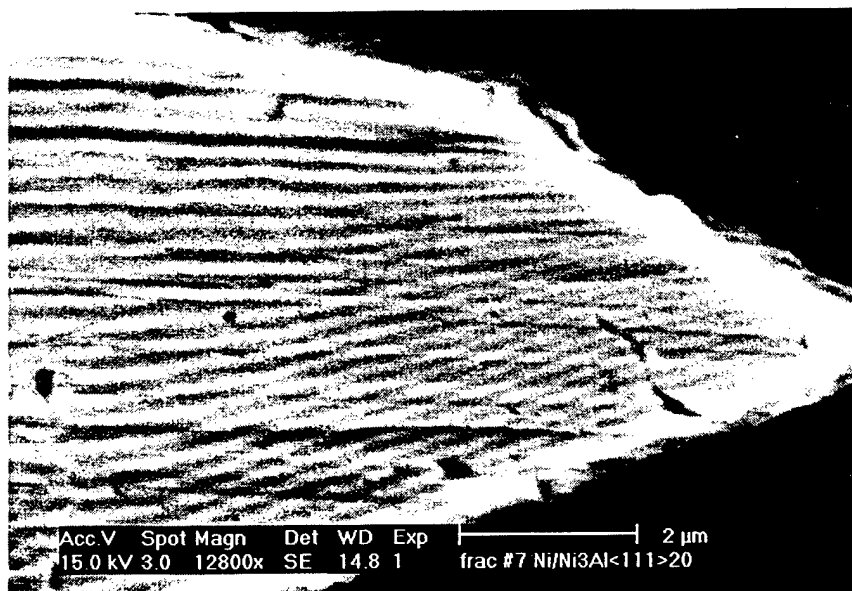

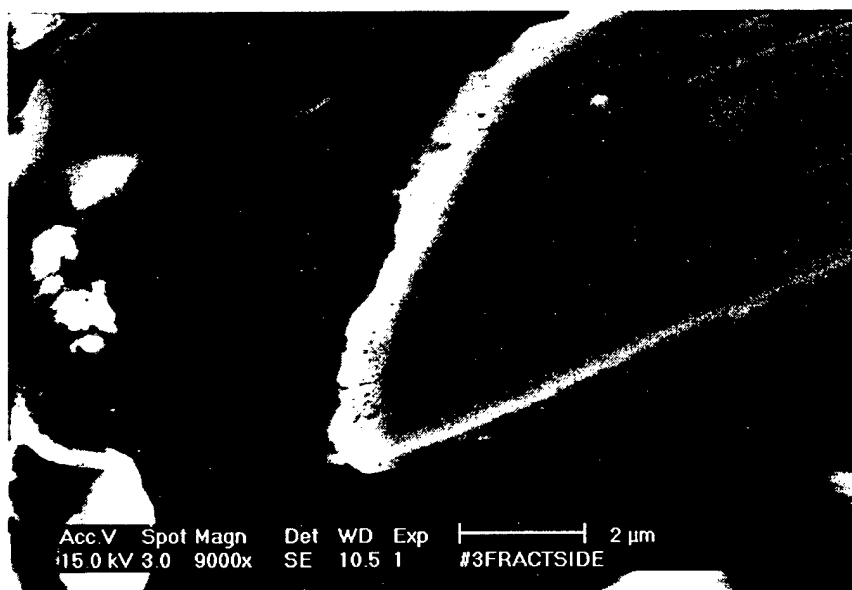Fig. 18:   SEM micrograph of the side view of a fractured <001> 120nm/120nm Ni/Ni$_3$Al multilayered sample (#4-7).

Fig. 19:   SEM micrograph of the side view of a fractured <001> 20nm/20nm Ni/Ni$_3$Al multilayered sample (#3-2).
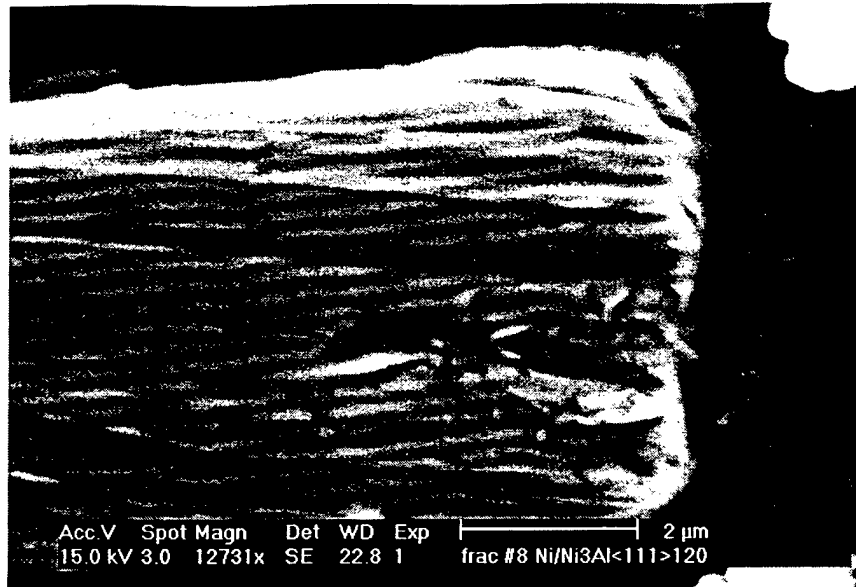
Fig. 20:   SEM micrograph of the side view of a fractured <111>
            120nm/120nm Ni/Ni$_3$Al multilayered sample (#8-4).
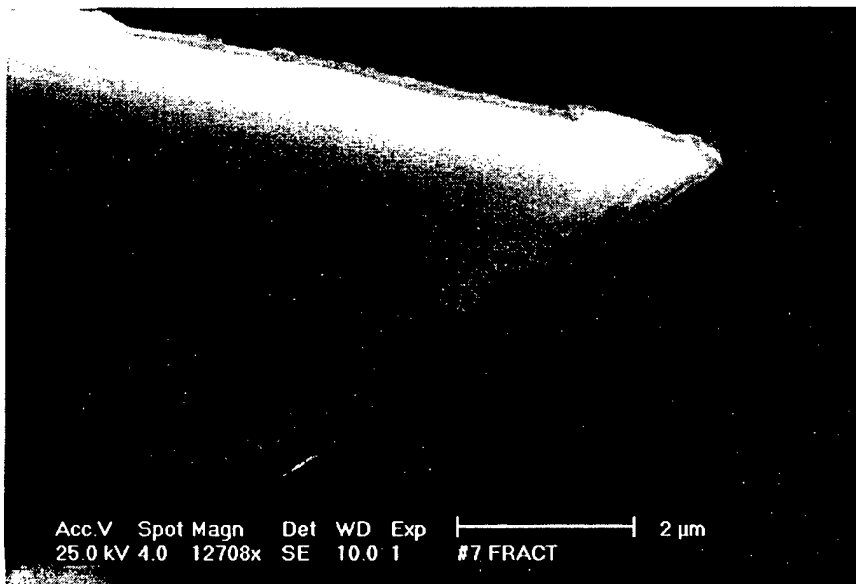
Fig. 21:   SEM micrograph of the side view of a fractured <111>
            20nm/20nm Ni/Ni$_3$Al multilayered sample (#7-1).

e. Observation of critical strength dislocation configurations in
   multilayered thin films
        Collaboration with Dr. Tim Foecke involved in-situ TEM straining
   experiments to identify critical deformation mechanisms that control
   strength of such materials. His observations of slip in the model
   Cu/Ni multilayer identified a critical deformation process shown in
   Figure 22, in which dislocation loops encounter resistance to

propagation into adjoining layers, due to misfit dislocations positioned along interfaces. The critical event identified is the transmission of the leading (N = 1) dislocation across the interface.
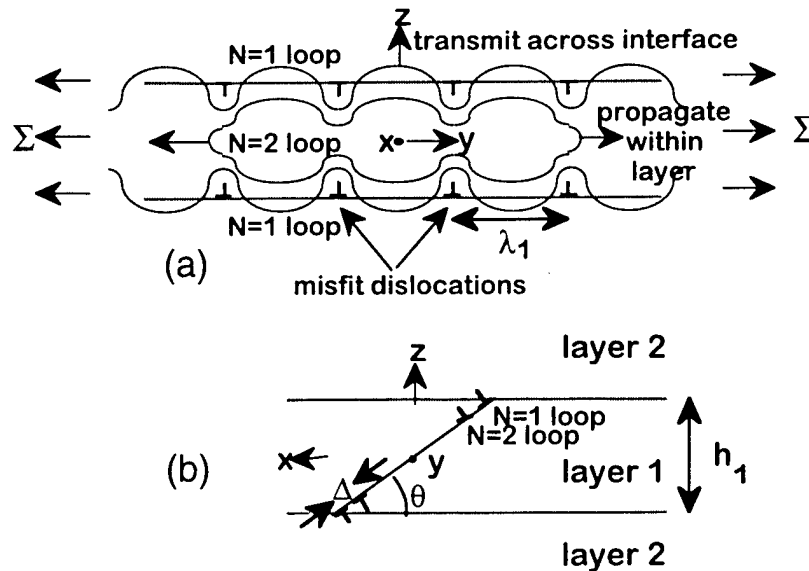

Figure 22: Schematic showing a dislocation pile-up configuration, as motivated by *in situ* TEM strain studies of a model system of Cu/Ni metallic multilayers. Misfit dislocations at the interface act as obstacles to the propagation of slip from type 1 layers into adjoining type two layers [6]. Note the two competing modes of loop propagation within a layer, versus loop transmission across an interface.

A second common observation was the occurrence of a peak strength or hardness at a critical layer thickness. For example, **Figure 23** shows data from Lehoczky [3] for 50%Cu-50%Al multilayers, in which yield strength is observed to reach a peak when layer thickness is approximately 50nm. Independent hardness data from Lankey [2,3] shows a plateau in strength at thickness below 50nm. This phenomenon has been observed in several systems, even including NbN/X multilayers, where X may be a metal such as Mo or W, or another nitride such as TiN [7, 8]. In these cases, peaks in hardness are observed for layer thickness in the range of 2 to 8 nm.
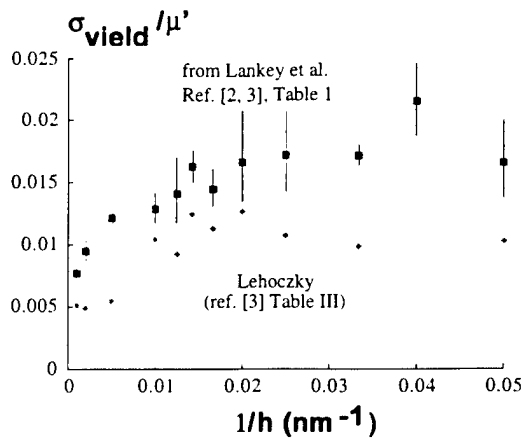
Figure 23: Values of yield strength in 50%Al/50%Cu multilayers as a function of layer thickness, h, taken from [5]. The data was obtained from tensile test results by Lehoczky [3] and from indentation test results by Lankey [1, 2].

f. Corresponding modeling of strength of multilayered thin films

The goal of this effort wass to predict the strength of multilayered thin films as a function of layer thickness, lattice mismatch, and resistance of the interface to transmission of dislocations, based on the physical process slip pile-up shown in Figure 22. Thus, the model incorporates the physical features in Figure 22 and the model results are significant since they identify a reason why multilayered materials may display a peak strength as a function of layer thickness.

A reason for peak strength identified here is that a decrease in layer thickness can decrease the density, $1/\lambda_l$, of misfit dislocations and thus decrease the resistance of the interface to transmission of the leading, $N = 1$, glide dislocation. In particular, **Figure 24** shows that larger values of local stress (σ_{misfit}) are required to produce a given density of misfit dislocations as layer thickness is decreased. **Figure 25** shows that the equilibrium density of misfit dislocations can be expressed as a function of the macroscopic applied stress, Σ, and ratio, a_2^o/a_1^o, of stress-free lattice parameters of the two phases. Thus, the strength of interfaces to transmission is inherently a function of applied stress, stress-free lattice parameters, and layer thickness.
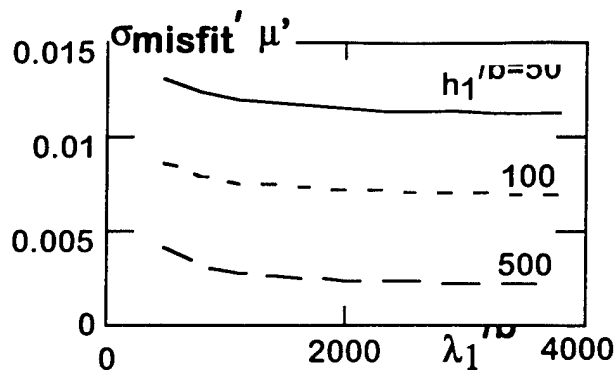
Figure 24: In-plane stress in type 1 layers necessary to introduce misfit dislocations in layer 1, as a function of the spacing λ_1 of existing misfit dislocations and layer thickness h_1 (= h_2). The elastic shear modulus is _, and the magnitude of the Burgers vector is b.

Figure 25: Macroscopic in-plane stress necessary to form misfit dislocations in layer 1, as a function of lattice parameter mismatch, for fixed layer thickness h_1/b = h_2/b = 100.

Figure 26: Resolved shear stress necessary to transmit the leading (N = 1) dislocation loop in Figure 3 across the interface from layer 1 to layer 2, as a function of the number, N, of loops. Layer thickness h_1/b = h_2/b = 50, 100, 500.

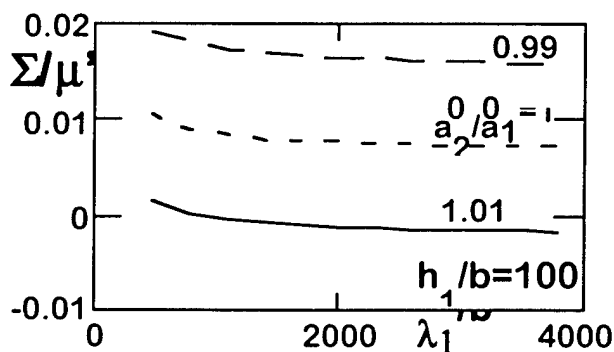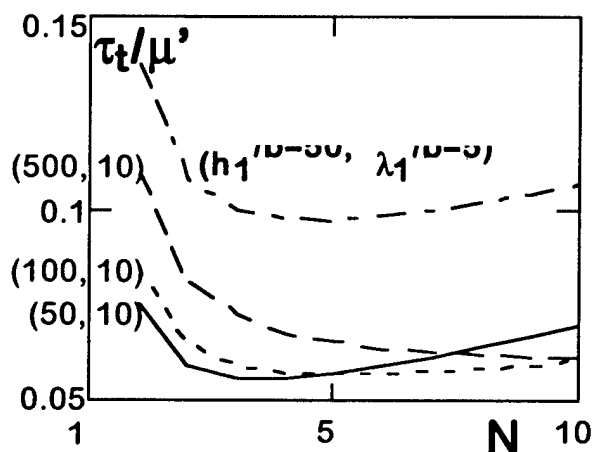**Figure 26** underscores that the critical stress to transmit the leading dislocation increases as the misfit dislocation density increases. However, it also shows how the critical stress depends on the layer thickness and number, N, of dislocations in the pile-up. This prediction was produced from a linear-elastic analysis of dislocation pile-ups in alternating layers of a multilayered thin film.

Figure 27 documents the increase in resolved shear stress to propagate new dislocation loops within the layer (i.e., along the x_1-direction in Figure 3) as a function of the number, N, of dislocations in the pile-up and thickness, h_1, of the layer in which they
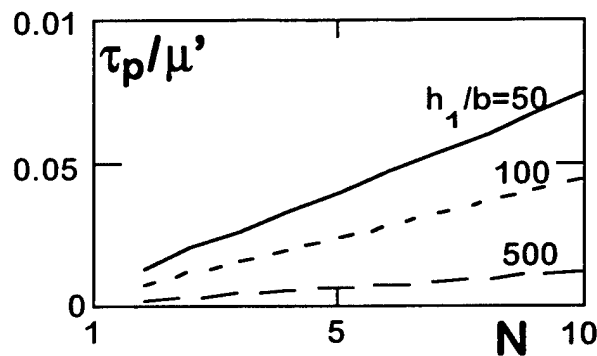
Figure 27: Resolved shear stress necessary to propagate dislocation loops within layer 1, as a function of loop number N. Layer thickness $h_1/b = h_2/b = 50, 100, 500$.

propagate. Thus, multilayers with smaller layer thickness require larger increases in resolved shear to add another loop onto a pile-up.

The distinct elements of the analysis, as presented in Figures 24-27, are combined to predict the critical macroscopic stress required for transmission of the leading (N = 1) dislocation in the pile-up. **Figure 28** shows the predictions for two cases in which there is no lattice mismatch ($a_2^o/a_1^o = 1$) versus a 1% lattice mismatch ($a_2^o/a_1^o = 0.99$). The lattice mismatch dramatically lowers the macroscopic stress for transmission in this case.

Σ/μ' for transmission

$\tau_i^0/\mu'=0.01$

$a_2^0/a_1^0 = 1$

$a_2^0/a_1^0 = 0.99$

$h_1{}^{\prime o}\left(=h_2{}^{\prime o}\right)$

Figure 28: Macroscopic stress to transmit the leading dislocation in a pile-up from layer 1 into layer 2, versus layer thickness, for $a_2^0/a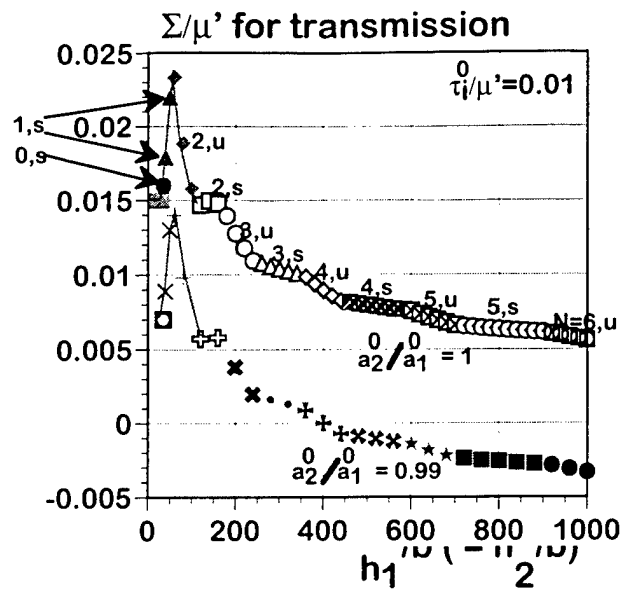_1^0$ = 1 and 0.99. The number, N, next to each symbol group denotes the number of pile-up dislocations at transmission. The resistance of a coherent interface to transmission is $\tau_i^0/\mu'=0.01$ and h_1 = h_2 is used.

The analysis shows a large regime in which the macroscopic yield stress increases as layer thickness is decreased. This regime is also observed in the data shown in Figure 23. The increase in yield stress is predicted since an increased stress is needed to propagate dislocations in thinner layers, as noted in Figure 27, and since the density of misfit dislocations is relatively large and does not change dramatically with layer thickness in this regime. Noted at various points along the upper curve is the number of dislocations in the pile-up when the leading (N = 1) dislocation transmits across the interface. Thus, the model predicts that the number of dislocations in the pile-up at transmission decreases with decreasing layer thickness.

At even smaller values of layer thickness, the yield strength reaches a peak. For the parameters considered here, the peak occurs for layer thickness in the vicinity of 50 to 75 b, which corresponds to 10 to 25 nm for copper, for example. The peak occurs since in this vicinity of layer thickness, the density of misfit dislocations dramatically decreases and thereby reduces the strength of the interface to transmission.

We note in a recent publication [9] that the basic dislocation propagation mode may change in the vicinity of this peak, since the stress to transmit a dislocation loop across an interface may become comparable to that to propagate a dislocation loop within a layer.

The features of this model provide numerous points for comparison to experimental TEM work and mechanical testing.

g. <u>Modeling the competition between yield and fracture</u>

The current state of modeling of the critical macrostress for macroyield of layers, as described above, is summarized in **Fig. 28**. Here, the macrostress for transmission monotonically increases with decreasing layer thickness up to a critical thickness, below which the macrostress falls off. This critical thickness is associated with a transition from semicoherent interfaces at larger layer thickness to coherent interfaces at smaller layer thickness. X-ray diffraction measurements have documented such a transition in <001> fcc-Ni/γ'-Ni$_3$Al multilayers, in the range of 20nm to 120nm layer thickness.

Corresponding modeling of confined layer fracture modes, shown in **Fig. 29**, suggests that the macrostress to drive the fracture process also increases with decreasing layer thickness, h, according to

$$\sigma_{f(CLF)} = \sqrt{\frac{E_i}{C(1-v_i^2)}} \left(\sqrt{\frac{G^*}{h}} + \frac{\sqrt{2\Psi}}{h} \right). \tag{1}$$

where G* is the critical energy release associated with fracturing the brittle (γ') layers and Ψ is the additional energy consumed by trailing debonding zones or by trailing lines of plasticity that are expected to occur in the adjoining ductile (fcc-Ni or γ-Ni(Al)) layers (**Fig. 29**). Eq. (1) indicates that there are energetic reasons why the stress to drive confined layer fracture is expected to increase with decreasing layer thickness.
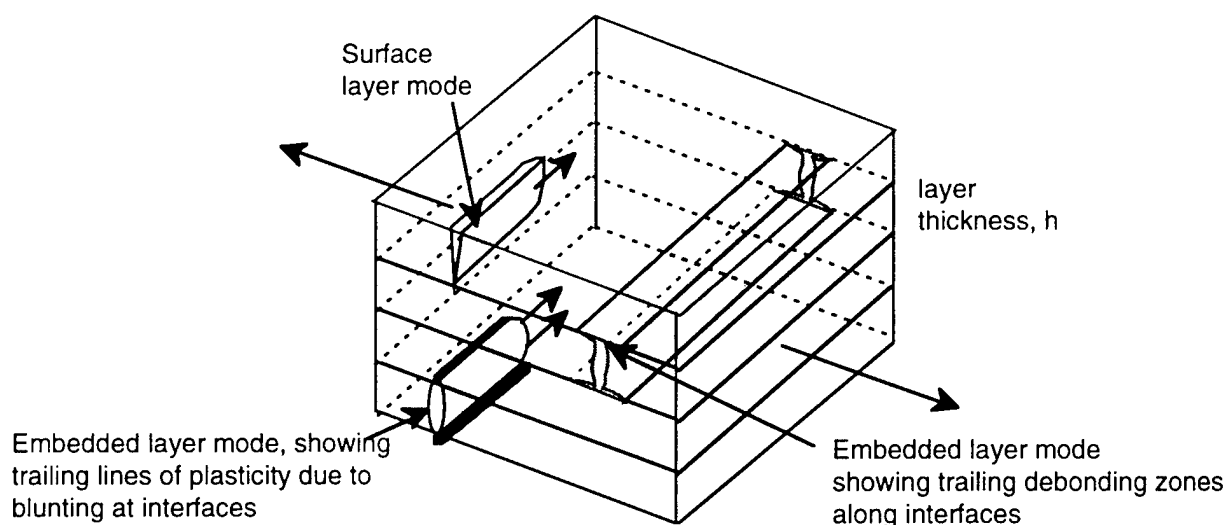

Fig. 29:   Examples of confined layer fracture in layered composite materials.

The competition between confined layer fracture and macroyielding is represented schematically in **Fig. 30**. There, the macrostress for yield and that for confined layer fracture both increase with decreasing layer thickness. The results of SEM fractography suggest that, over the range of layer thickness and epitaxies considered, the yield and fracture curves are positioned so that yield before fracture occurs for the <001> epitaxy cases. However, the results are mixed for the <111> epitaxy, with the 120nm/120nm case falling in the fracture before macroyield regime and the 20nm/20nm case falling into a borderline regime.

The relative positions of the <111> and <001> macroyield curves depends, in part, on the nature of the interfaces in each epitaxy and the ability of those interfaces to confine slip to within individual layers. An increase in the interfacial resistance to slip transmission would displace the macroyield curve upward. The schematic in **Fig. 30** suggests that interfacial slip transmission may be more difficult in the <111> epitaxy than in the <001> case.
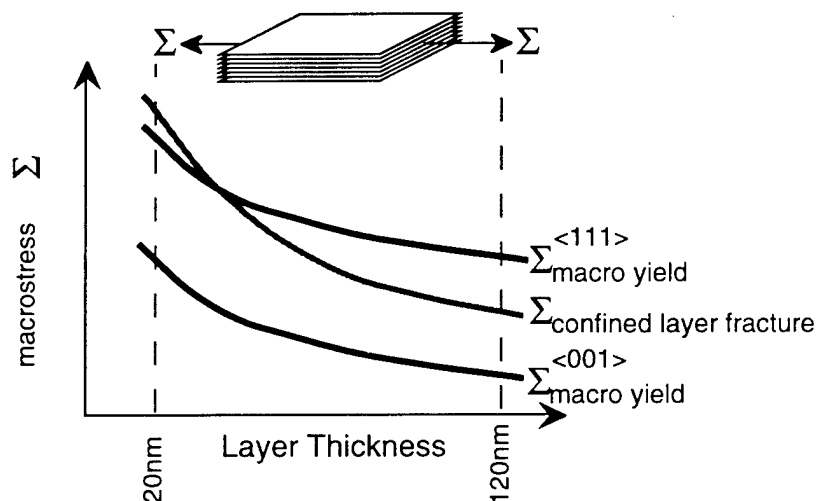
Fig. 30: Schematic of the competition between confined layer
          fracture and macroyield involving transmission of
          dislocations across interfaces, as a function of layer
          thickness and epitaxy.

h. Fracture resistance and R-curve behavior in multilayered materials

During the past year, we completed an analysis of the effect of microcracking on the fracture resistance of two-phase multilayered materials. The intended application is to understand how profuse microcracking in the vicinity of a macrocrack may arrest propagation of the macrocrack. The analysis includes the effects of volume fraction and thickness, fracture toughness, and flaw content of the individual layers. **Figure 31** shows the results for 2D macrocrack propagation through a multilayered composite, and indicates the formation of a microcrack at each location where there is a number.

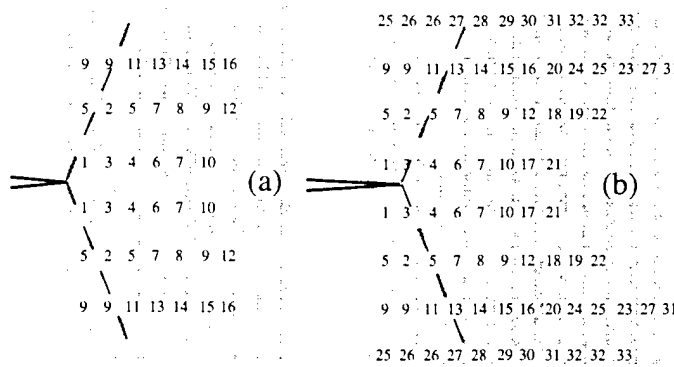The number also indicates the order of microcrack nucleation during

Figure 31: Predictions of microcracking in the vicinity of a macrocrack propagating in a two-phase layered material for (a) the onset of macrocrack growth and (b) after macrocrack growth.
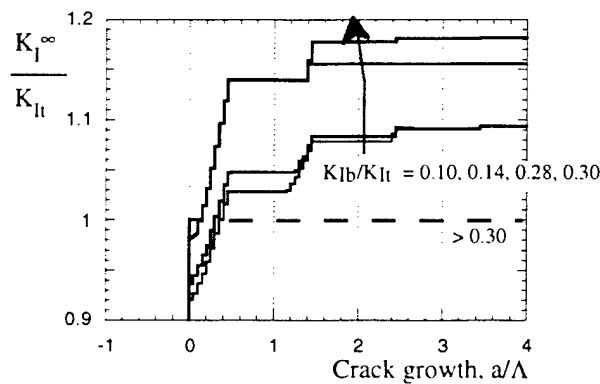

Figure 32: Predicted crack growth resistance curves for two-phase multilayered samples, where subscripts "b" and "t" refer to the brittle and tougher phases, respectively, and Λ is the bilayer dimension.

advance of the macrocrack. Sample crack growth resistance curves from the analysis are displayed in **Figure 32**.

Principal conclusions from this effort are that increasing the density of flaw sites, the bi-layer thickness, and the difference in moduli of the two phases are predicted to increase the steady state fracture toughness generated by microcracking. The largest R-curve plateaus produced for the range of parameters considered here are about 1.3 times the fracture toughness of the tougher phase. However, both the model and experimental results in the literature suggest that much larger R-curve plateaus can be obtained when the macrocrack tip is blunted or deflected by interfacial cracking.

These observations may be coupled with the statement in the progress report from last year that the fracture stress is proportional to (fracture toughness)x(crack length)$^{-1/2}$. In carefully produced multilayered samples, the prevailing crack length in an "as-is" multilayer is expected to correspond to the layer thickness, so that a decrease in layer thickness is expected to increase fracture strength. However, the modeling presented suggests that fracture

toughness from microcracking (and presumably also from plasticity) will decrease with decreasing layer thickness. For this reason, the fracture strength, like yield strength, may not monotonically increase with decreasing layer thickness but may reach a peak with decreasing layer thickness. Planned tensile tests on free-standing thin films will help to address this issue.

i. Morphological stability of γ-Ni(Al)/γ'-Ni$_3$Al multilayered thin films

Figures 33 to 36 display the SEM micrographs of polished γ-Ni(Al)/γ'-Ni$_3$Al samples after heating at 800C for 101 hours. The results indicate that all multilayers tested show the tendency for layers to pinch off. This is evident in **Fig. 33**, where layers are pinched off at several locations. An overall comparison reveals that, for a given epitaxy, 20nm/20nm multilayers suffer this instability more rapidly than 120nm/120nm multilayers. Further, the <111> epitaxy cases display more rapid instability than <001> cases with comparable layer thickness. Thus, the <001> 120nm/120nm case was the most resistant to pinching off while the <111> 20nm/20nm was the least resistant.

The <001> 20nm/20nm micrograph (**Fig. 34**) is unique among those shown, in that morphological breakdown resembles a cuboidal particulate microstructure. Significant coarsening of grains has occurred, since average particle size is many times the 20nm dimension of the individual layers from which they were produced.

Fig. 33: Morphology of <001> 120nm/120nm γ-Ni(Al)/γ'-Ni$_3$Al multilayer after heating to 800C for 101hours (#11-10).

Fig. 34:   Morphology of <001> 20nm/20nm γ-Ni(Al)/γ'-Ni₃Al
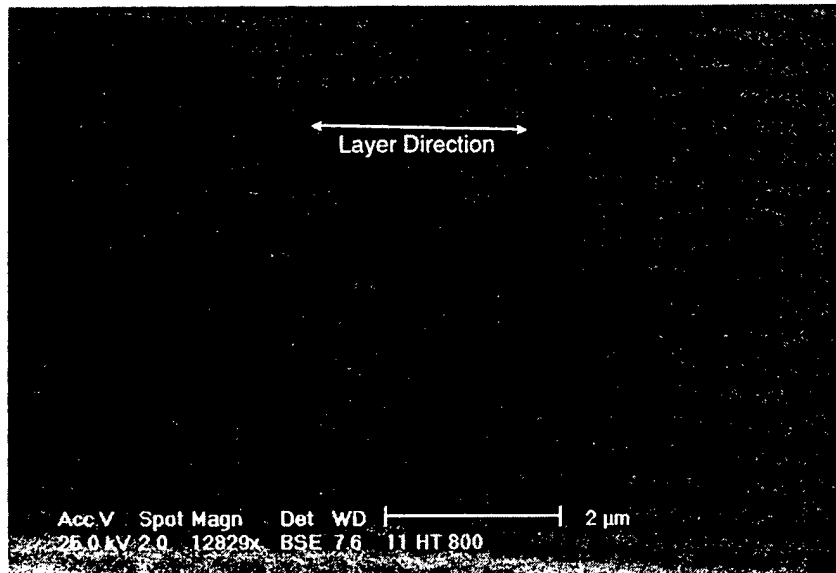   multilayer after heating to 800C for 101hours (#13-3).
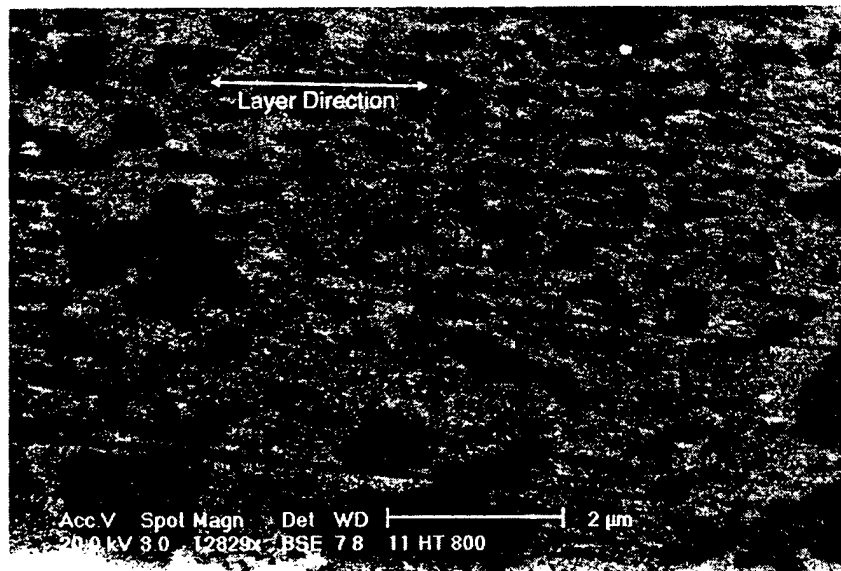

Fig. 35:   Morphology of <111> 120nm/120nm γ-Ni(Al)/γ'-Ni₃Al
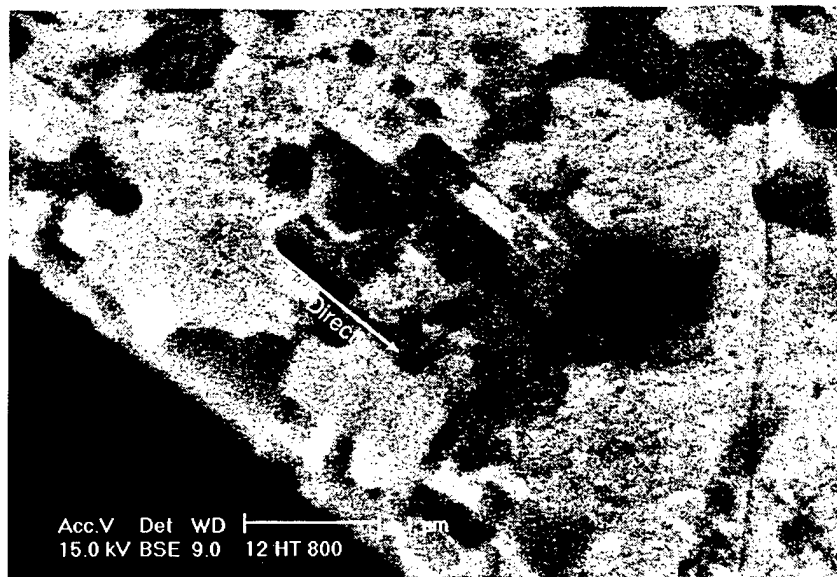   multilayer after heating to 800C for 101hours (#10-4).

24/24

Fig. 36:   Morphology of <111> 20nm/20nm γ-Ni(Al)/γ'-Ni$_3$Al
multilayer after heating to 800C for 101hours (#12-7).

j. Modeling of morphological stability of thin films

We collaborated with Dan Josell at NIST to model morphological
instability caused by pinching off of layers as depicted in **Fig. 37**.
The model seeks the equilibrium grooving angle for a particular set of
interfacial and grain boundary energies while holding the volume of
individual grains constant. The columnar grains in the model are
described by a height, t, and an in-plane width, w.

Fig. 38 shows predictions of the modeling for γ-Ni(Al)/γ'-Ni$_3$Al
multilayers with columnar grains. The plots adopt grain boundary
energies of 866 and 902 mJ/m^2, as estimates for the Ni(Al) and
Ni$_3$Al phases, respectively. Stable and unstable regions to pinching
off of Ni$_3$Al layers are identified as a function of grain aspect
ratio, t/w, and energy, γ_i, of the Ni(Al)-Ni$_3$Al interface.
Multilayers with larger t/w and larger γ_i are more likely to be stable
to pinching off. Equivalently, if interfacial energy is decreased,
only multilayers with larger values of t/w (i.e., more needle-like
columnar grains) are stable to pinching off. Ultimately, there is a
critical value of γ_i, equal to 18mJ/m^2 in this case, below which no
multilayer morphology is stable.

For application to the multilayers at hand, the 20nm/20nm
multilayers are expected to have smaller interfacial energies than
120nm/120nm multilayers. This occurs since interfaces in the
20nm/20nm cases are expected to be more coherent, with fewer misfit
dislocations, than interfaces in the 120nm/120nm cases. Estimates of
γ_i for the <001> case range from 10 to 20 mJ/m^2 for coherent
interfaces to 200 mJ/m^2 for semi-coherent interfaces, as studied in
rafted morphologies. Thus, according to **Fig. 38**, fine multilayered
samples are expected to lie on the left side of the plot where
interfacial energies are small and where stability is predicted only
for extremely large values of t/w (i.e., needle-like grains).
Alternately, multilayers with larger layer thickness are expected to
lie on the right side of the plot, where interfacial energies are

larger and where stability is predicted for a large range of t/w, from pancake to needle-like grains.
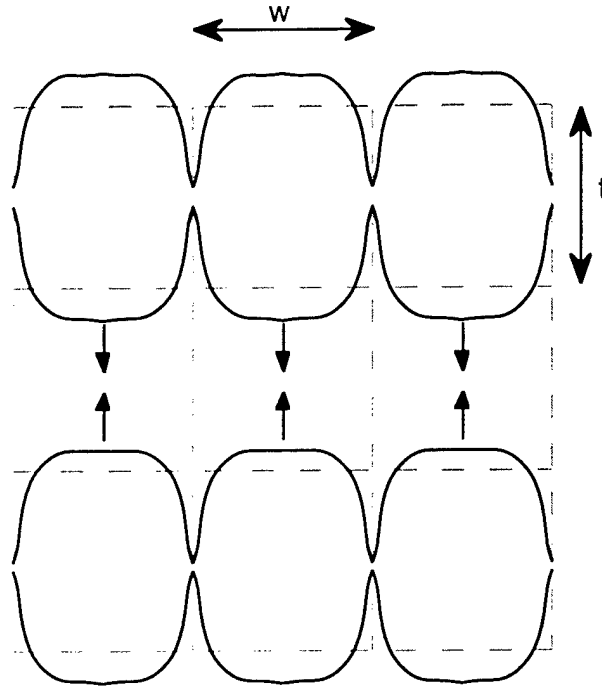
Fig. 37: Pinching off of alternating layers due to a difference in the energy of columnar grain boundaries between the γ-Ni(Al) and γ'-Ni$_3$Al phases. The light gray dashed lines indicate the positions of interfaces and columnar grain boundaries prior to pinching off. The dimensions w and t are the in-plane and out-of-plane dimensions of the individual columnar grains.
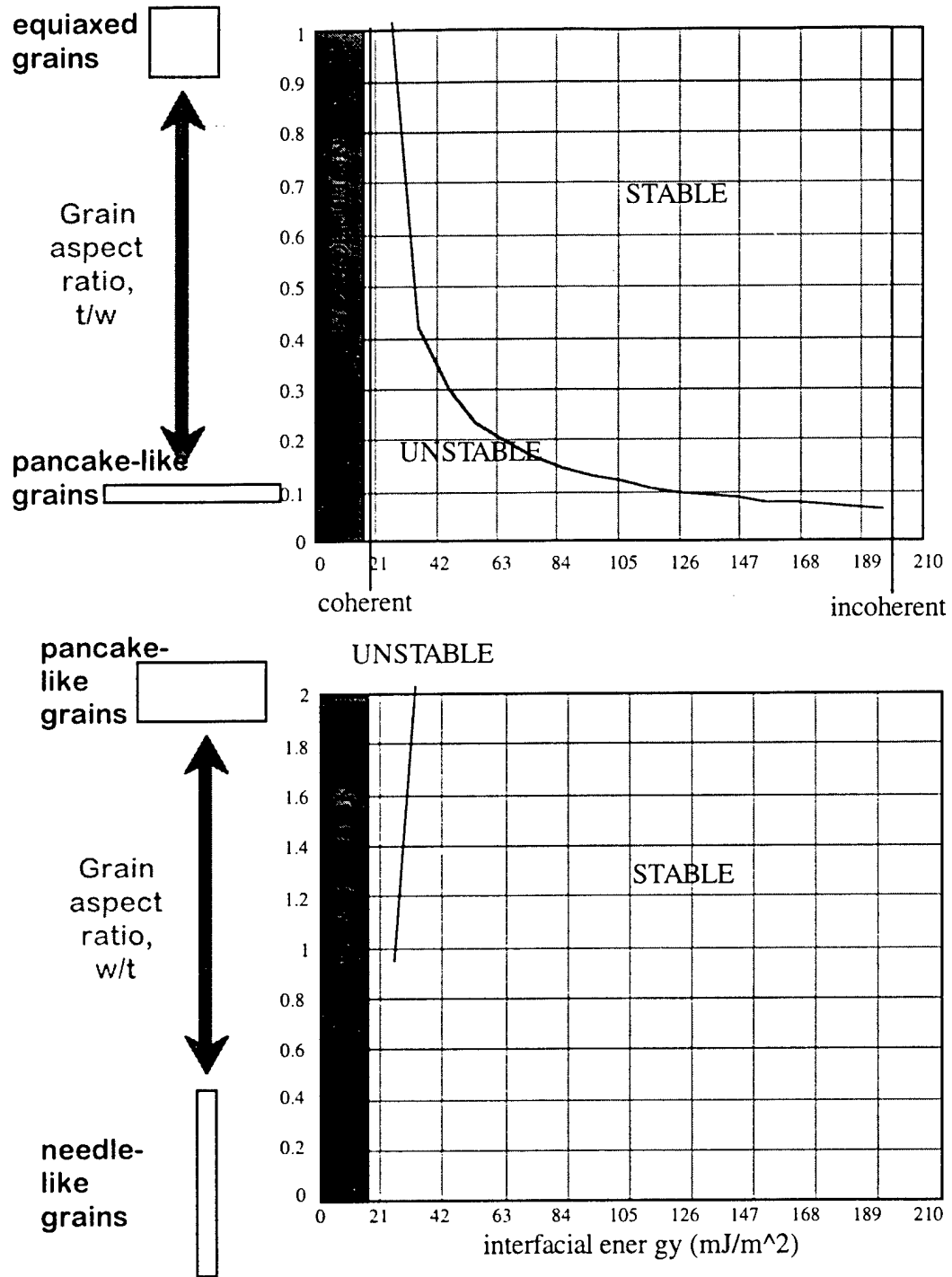
Fig. 38: Stability diagrams for pinching off of γ'-Ni$_3$Al layers in γ-Ni(Al)/γ'-Ni$_3$Al multilayered samples, based on columnar grain boundary energies of 866 and 902 mJ/m^2 for γ-Ni(Al) and γ'-Ni$_3$Al layers, respectively.

27/27

k. Inherent resistance of non-slipping interfaces to dislocation transmission

During the last year, we developed a computational technique that furnishes the critical resolved shear stress for dislocation transmission across an interface, as a function of the mismatch in elastic moduli across the interface, and in terms of the bonding properties across the candidate slip planes on each side of the interface. This activity is a stated goal in the original AFOSR proposal and is an important activity to understand the mechanical response of interface-dominated materials such as Ni/Ni$_3$Al multilayers. The analysis is confined to the case of co-planar slip planes, with the Burgers vector parallel to a coherent interface, and the limiting case of a non-slipping interface is studied. This simple geometry provides revealing information about how relative bonding properties and modulus mismatch affect the interfacial resistance to transmission.

Figure 39 displays a sample result showing how the resolved shear stress, τ, to hold the dislocation at a distance c from the interface increases as c is decreased. Here, distance is measured in units of dislocation Burgers vector magnitude, b, and the shear stress is normalized by $\kappa_\mu\mu$, where $\kappa_\mu = (\mu_2 - \mu_1)/(\mu_2 + \mu_1)$ and μ is the elastic shear modulus (μ_1 or μ_2) of the phase in which the dislocation approaches the interface. The results show how the present model, denoted by "Current formulation" compares to earlier, less physical approaches by Pacheco & Mura (1969) and Head (1953). The comparison here is for a simple Frenkel sinusoidal relation for the atomic shear stress-relative shear displacement across the interface, as depicted by curve "C1" in **Figure 40**.
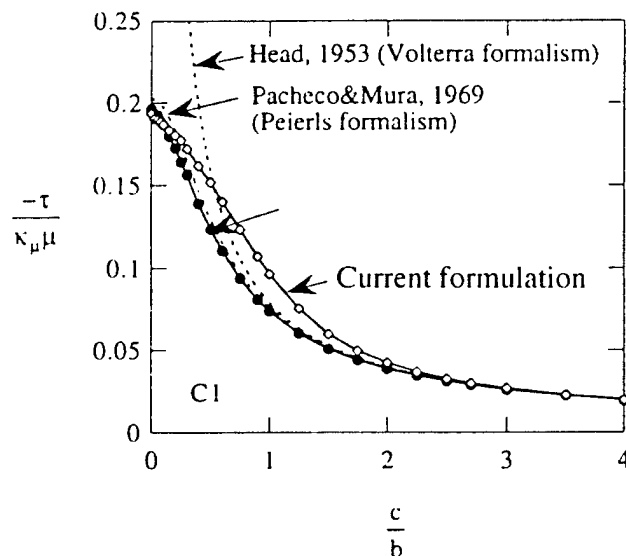

Figure 39: Comparison of the resolved shear stress needed to hold a screw dislocation at a distance, c, from an interface, as predicted by the original Head formalism, the approximate Peierls solution of Pacheco and Mura, and the current formulation employing a Beltz and Rice formalism.

	$\overline{\gamma}_{us}$	$\overline{S}_{max}$
C1:	1	1
C2:	0.8	1
C3:	0.8	0.8233
C4:	0.5	0.5
C5:	1	1 (2nd set)
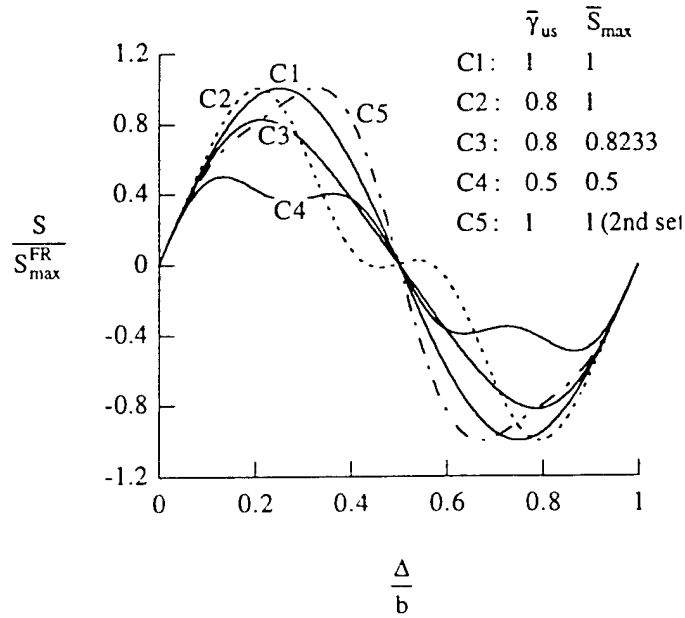
Figure 40: Various shear stress-relative shear displacement relations considered for candidate slip planes. γ_{us} is the unstable stacking fault energy and S_{max} is the peak shear stress in the relation.

Figure 41 extends previous formalisms by showing how the resolved shear stress to push a dislocation through an interface changes with the various bonding relations considered in Figure 40. The conclusions developed thus far from the work are that the critical shear stress for transmission scales linearly with the unstable stacking fault energy, which is the maximum energy that can be stored per unit area of slip plane, as that plane is uniformly sheared; in contrast, the critical shear stress depends very weakly on the peak shear stress in the slip plane bonding relations shown in Figure 40.
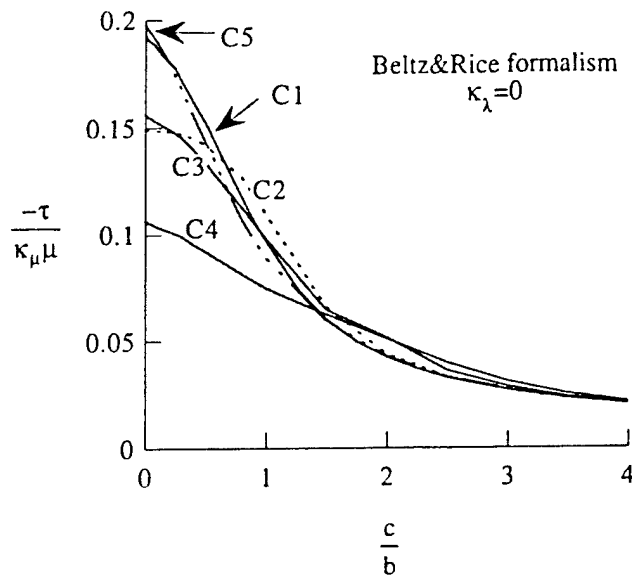
Figure 41: Predictions of the resolved shear stress to hold a screw dislocation at a distance, c, from an interface, for the various shear stress-relative shear displacement relations shown in Figure 40.

The formalism has also been extended to include different bonding relations on either side of the interface and those implications are being explored further. Additional effort is underway to extend the formalism to non-coplanar slip planes, so that particular slip geometries in the <111> and <100> epitaxies, as identified in **Figure 42(a)** and **(b)**, respectively, can be studied.
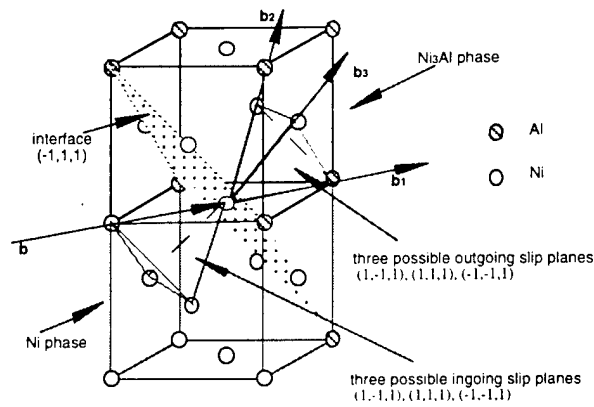
Figure 42: Slip plane geometries identified for the (a) <111> and
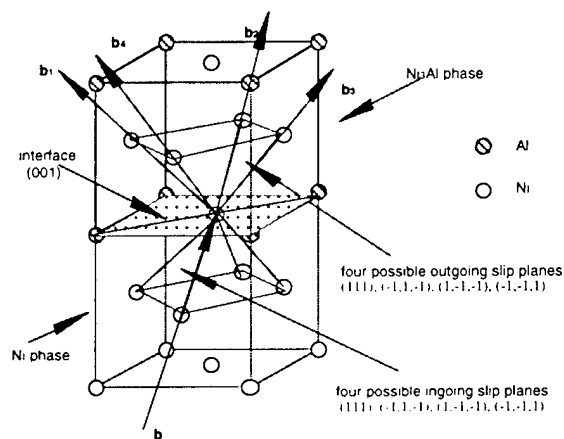
(b) <100> epitaxial orientations in Ni/Ni$_3$Al multilayers.

1. Inherent resistance of slipping interfaces to dislocation transmission

One of the key material parameters needed to understand nanolayered composites is the resistance of interfaces to slip transmission. Hazzledine and Rao at UES, Inc. have summarized several important contributions to the critical stress for interfacial slip transmission, including dislocation core spreading into the interface, mismatch in elastic moduli between layers, differences in stacking fault energy between layers, ordering mismatch associated with a unit dislocation in one layer becoming a partial dislocation and dragging an antiphase boundary into the second layer, and creation of a residual dislocation at the interface, due to different Burgers vectors in the two layers.

The previous development of a Peierls model, as summarized in the previous section, included the second and third effects mentioned above. In order to include the first effect, we extended that Peierls modeling to include potential shearing of the interface as the dislocation passes from one layer to another. The analysis is limited

to interfacial transmission of a screw dislocation with Burgers vector parallel to the interface plane, in a two-dimensional geometry.
Figure 43 shows a sample slip distribution predicted by the model, as a screw dislocation passes across an interface.

   A significant, initial observation is that, if the interface is made more compliant to shearing, then the peak shear stress required to drive the dislocation across the interface can increase dramatically. In particular, reduction in the stacking fault energy associated with slip in the interface can produce significant core spreading in the interface. In that case, the critical step in the transmission process requiring the peak stress is the contraction of the core back onto the outgoing slip plane.
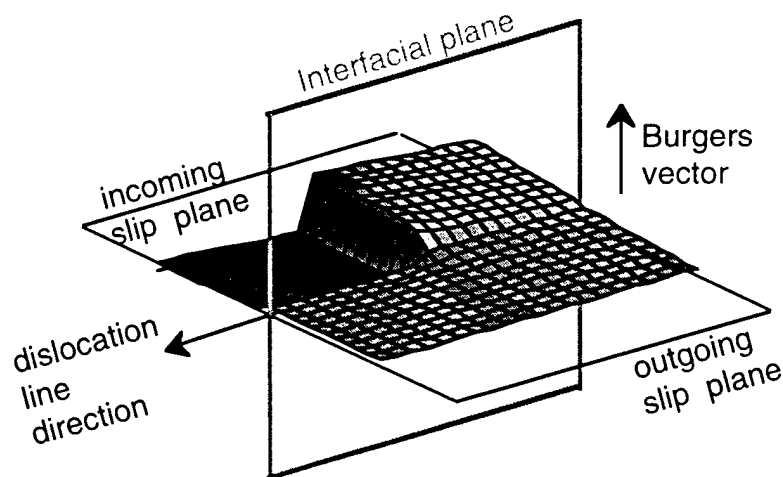
Fig: 43:   An example of a slip profile during the incremental
           passage of the screw dislocation across an interface,
           showing core spreading in the interfacial plane.

   This extension of the slip transmission model has yet to be applied to the γ-Ni(Al)/γ'-Ni$_3$Al system in particular.

References
1. R.L. Lankey, L.M. Hsiung, H.N.G. Wadley, S.M. Karecki, D.T. Smith, B.L. Halpern, and J.J. Schmitt, Material Research Symposium Proceedings, 382 (1995), 113.
2. S.L. Lehoczky, Journal of Applied Physics, 49 (11) (1978), 5479.
3. S.L. Lehoczky, Physical Review Letters, 41 (26) (1978), 1814.
4. R. Ahuja, Ph.D. Thesis, The Ohio State University, 1996.
5. E.R. Kreidler, Jr., "Orowan-Based Deformation Models for Multilayered Materials" (M.S. thesis, Ohio State University, 1997).
6. Anderson, P.M., and Foecke, T., Slip propagation in metallic multilayered thin films, to be presented at the Fall Meeting of TMS, October 11-15, 1998.

7. Scott A. Barnett, private communication with author, Northwestern University, April 21, 1998.
8. M. Shinn, L. Hultmann, and S.A. Barnett, Journal of Materials Research, 7 (4) (1992), 901.
9. Peter M. Anderson and Eric R. Kreidler, Jr., <u>Materials Research Society Symposium on Thin Films: Stresses and Mechanical Properties</u>, MRS Fall Meeting, Dec. 1-5, 1997.

5. Personnel Supported

a. Graduate Students

Yaogeng Cheng	(1 Sep 97 to 30 Jun 99)
Eric Kreidler Jr.	(1 Jul 96 to 1 Sep 97)
Gregory Thompson	(1 Jul 96 to 31 May 97)
Amancherla Sundar	(1 Sep 97 to 30 Jun 99)
Katrin Schwendner	(1 Sep 98 to 30 Jun 99)

b. Post-doctoral Researchers

Rajarshi Banerjee	(1 Aug 98 to 30 Jun 99)	
Xiaodong Zhang	(1 Jan 97 to 30 Jul 98)	
	(1 Aug 98 to 30 Jan 99)	(1/2 appt)
Xiao Xin	(1 Jun 97 to 30 Aug 98)	(1/2 appt)

c. Faculty (OSU)

Peter Anderson	(1 Aug 96 to 31 Aug 96)
	(1 Aug 97 to 1 Sep 97)
Hamish Fraser	(1 Aug 96 to 31 Aug 96)
	(1 Aug 97 to a Sep 97)

d. Unsupported Collaborators

Peter Hazzledine, Ph.D.	UES, Inc.
Satish Rao, Ph.D.,	UES, Inc.
Daniel Josell, Ph.D.,	NIST
Timothy Foecke, Ph.D.	NIST

6. Publications

Banerjee, R., Thompson, G.B., Zhang, X.D., Anderson, P.M., and Fraser, H.L., "Development of Texture and Order in Sputter Deposited Ni_3Al Thin Films," manuscript in preparation, 2/00.

Xin, X.-J., and Anderson, P.M., "A Peierls Approach to the Critical Shear Stress for Dislocation Transmission Through a Bimaterial Interface," manuscript in preparation, 2/00.

Anderson, P.M. and Xin, X. "A Peierls Approach to the Critical Shear Stress for Dislocation Transmission Through a Bi-material Interface", J.R. Rice 60th Anniversary Vol. (J. Chuang, ed.,) Kluwer Publishers, Dordrecht (2000).

Anderson, P.M., and Shewmon, P.G., "Stress Redistribution and Cavity Nucleation near a Diffusively Growing Grain Boundary Cavity," accepted in **Mechanics of Materials**, 2/00.

Fain, Jason P., Banerjee, R., Josell, D., Anderson, P.M., Fraser, H., Tymiak, N., Gerberich, W.W., "Morphological Stability of $Ni(Al)/Ni_3Al$ Nanolaminate Composites", MRS Symp. Proc. on Nanophase and Nanophase Composites III" (S. Komarneni, J.C. Parker, and H. Hahn, eds.), Boston, MA (1999).

Banerjee, R., Fain, J.P., Anderson, P.M., and Fraser, H.L., "Processing, Microstructure, and Fracture Behavior of Nickel/Nickel Aluminide Multilayered Thin Films", MRS Symp. Proc. on Thin Films--Stresses and Mechanical Properties VIII (R. Vinci, O. Kraft, N. Moody, P. Besser, E. Shaffer II, eds.), Boston, MA (1999).

Anderson, P.M., Rao, S., Cheng, Y., and Hazzledine, P.M., "The Critical Stress for Transmission of a Dislocation Across An Interface: Results from Peierls and Embedded Atom Models", MRS Symp. Proc. on Interfacial Engineering for Optimized Properties (C.B. Carter, E.L. Hall, C.L. Briant, and S. Nutt, eds.), Boston, MA (1999).

Anderson, P.M., Foecke, T., and Hazzledine, P.M., "Dislocation-based Deformation Mechanisms in Metallic Nanolaminates," **MRS Bull**. 24(2), 27 (1999).

Veress, A.L., Anderson, P.M., Cornhill, J.F., and Thomas, J.D., "Mechanical Response of an Artery Using a Standard Nonlinear Solid," Proc. Symp. Rocky Mountain Biological Society, April, 1998.

P.M. Anderson, "Microcrack toughening in two-phase multilayered composites," *Acta metall. et mater.* **46**(14) (1998). With S. Muju, and D.A. Mendelsohn.

P.M. Anderson, "Nucleation of Voids and Grain Boundary Cracking," *Acta metall. et mater.* **46**(14) (1998). With P. Shewmon.

P.M. Anderson, "Dislocation-based models of stress-strain behavior in multilayered thin films," Mater. Res. Symp. Proc. on Thin films: Stresses and Mechanical Properties, MRS Fall Meeting, Dec. 1-5, 1997. With E.R. Kreidler, Jr.

P.M. Anderson, "Mechanical Response of an Artery Using a Standard Non-linear Solid," Proc. 35th Rocky Mountain Bioengineering Symposium and 35th International ISA Biomedical Sciences Instrumentation Symposium, Copper Mountain, Colorado April 17-19, 1998. p. 212-217. With A.I. Veress, J.F. Cornhill, and J.D. Thomas.

P.M. Anderson, "Computer-based Interactive Modules using MathCad," to be published in *J. Materials Education* **20**(1,2) (1998).

Activation of Slip in Lamellae of a2-Ti3Al in TiAl Alloys, 1998, **Phil. Mag. A**, **78**, 217. With J.M.K. Wiezorek, X.D. Zhang and W.A.T. Clark.

Interaction of Dislocations and Interstitial Solute in g-TiAl, 1998, **Phil. Mag.A**, **77**, No. 3, 661. With J.M.K. Wiezorek.

Synthesis of BaAl2Si2O8 from Solid Ba-Al-Al2O3-SiO2 Precursors: II. TEM Analyses of Phase Evolution, 1996, Accepted, **J. Am. Ceram. Soc**.. With X-D Zhang and K. Sandhage.

Deformation Mechanisms in a Binary Ti-48Al Alloy with Lamellar Microstructure, 1997, **Philosophical Magazine Letters**, Vol. 75, No. 5, 271-280. With Jörg M. K. Wiezorek, Paul DeLuca and Michael J. Mills

Deformation and Fracture Characteristics in TiAl at room temperature and 800°C, 1997, **Matls. Sci. and Eng. A 234-236**, 1106-1109. With Jörg M. K. Wiezorek and Michael J. Mills.

Deformation Behavior of a2-Lamellae in Fully Lamellar Ti48Al-2Mn-2Nb at Room Temperature, 1998, **Scripta Materialia**, **38**, 811. With J.M.K. Wiezorek, X-D. Zhang, A. Godfrey, D. Hu, and M.H. Loretto.

Reaction between SiO2 and Molten Aluminum, 1998, **J. Japan Foundry Engineering Society**, **70**, 1. With K. Hoshino, T. Sugiyama, T. Kurosawa and T. Otani.

Precipitation of Ordered a2-Phase in Ti-6-2222, with X.D. Zhang, W.A. Baeslack III, D.J. Evans and J.M.K. Wiezorek, accepted for publication in **Acta Materialia**.

Polymorphic Phase Stability in Thin Multilayers, 1998, **Scripta Mater.**, **39**, 217. With S.A. Dregia and R. Banerjee.

Mechanisms of Plasticity and Fracture in Partially Lamellar TiAl at Room and Elevated Temperature, with P.M. With J.M.K. Wiezorek and DeLuca, submitted to **Acta Materialia**.

H.L. Fraser, HRTEM of Dislocations and Interfaces in TiAl, 1997, Mater. Res. Soc. Symp. Proc., **466**, 131-138. With M.J. Mills and J.M.K. Wiezorek.

H.L. Fraser, Determining directly from Experiment the Magnitude of the Burgers Vector of <c>-component Dislocations in Ti_3Al, 1997, *Phil. Mag. Letts*, Vol. **75**, No. 5, 281-289. With J.M.K. Wiezorek and C.J. Humphreys.

H.L. Fraser, Defect Sub-Structures in Lamellar Ti-48Al after 'Hard' Orientation Loading at Room and Elevated Temperature, 1997, 'Structural Intermetallics 1997', (TMS: Warrendale, PA), 195. With X.D. Zhang and J.M.K. Wiezorek.

H.L. Fraser, Observation of Ordered Ti3Al5 Precipitation in slightly Al-rich γ-TiAl, 1997, Microscopy and Microanalysis, **3**, Suppl. 2, 699. with S. Jayanthi, S. Swaminathan and J.M.K. Wiezorek.

H.L. Fraser, Microstructural Characterization and Mechanical Behavior of Novel In-Situ Be-Al Composites, 1997, 'Light Weight Alloys for Aerospace Applications IV', (TMS: Warrendale, PA), 247. With X.D. Zhang, G. Meyrick, F.C. Grensing and J.M.K. Wiezorek.

H.L. Fraser, Characterization of α_2-Precipitates in a (α/β) Titanium Alloy, 1997, 'Light Weight Alloys for Aerospace Applications IV', (TMS: Warrendale, PA, 173. With X.D. Zhang, W.A. Baeslack III, D.J. Evans and J.M.K. Wiezorek.

H.L. Fraser, Activation of Slip in Lamellae of α_2-Ti_3Al in TiAl Alloys, 1998, Phil. Mag. A, **78**, 217. With J.M.K. Wiezorek, X.D. Zhang and W.A.T. Clark.

H.L. Fraser, Interaction of Dislocations and Interstitial Solute in γ-TiAl, 1998, Phil. Mag.A, **77**, No. 3, 661. With J.M.K. Wiezorek.

H.L. Fraser, Synthesis of $BaAl_2Si_2O_8$ from Solid $Ba-Al-Al_2O_3-SiO_2$ Precursors: II. TEM Analyses of Phase Evolution, 1996, Accepted, J. Am. Ceram. Soc.. With X-D Zhang and K. Sandhage.

H.L. Fraser, Deformation Mechanisms in a Binary Ti-48Al Alloy with Lamellar Microstructure, 1997, Philosophical Magazine Letters, Vol. **75**, No. 5, 271-280. With Jörg M. K. Wiezorek, Paul DeLuca and Michael J. Mills

H.L. Fraser, Deformation and Fracture Characteristics in TiAl at room temperature and 800°C, 1997, Matls. Sci. and Eng. A **234-236**, 1106-1109. With Jörg M. K. Wiezorek and Michael J. Mills.

H.L. Fraser, Deformation Behavior of α_2-Lamellae in Fully Lamellar Ti48Al-2Mn-2Nb at Room Temperature, 1998, Scripta Materialia, **38**, 811. With J.M.K. Wiezorek, X-D. Zhang, A. Godfrey, D. Hu, and M.H. Loretto.

H.L. Fraser, Polymorphic Phase Stability in Thin Multilayers, Scripta Materialia, 1998, **39**, 217. With S. A. Dregia and R. Banerjee.

H.L. Fraser, Reaction between SiO_2 and Molten Aluminum, 1998, J. Japan Foundry Engineering Society, **70**, 1. With K. Hoshino, T. Sugiyama, T. Kurosawa and T. Otani.

H.L. Fraser, Precipitation of Ordered α_2-Phase in Ti-6-2222, with X.D. Zhang, W.A. Baeslack III, D.J. Evans and J.M.K. Wiezorek, accepted for publication in Acta Materialia.

H.L. Fraser, Mechanisms of Plasticity and Fracture in Partially Lamellar TiAl at Room and Elevated Temperature, with P.M. With J.M.K. Wiezorek and DeLuca, submitted to Acta Materialia.

7. Interactions/Transitions

a. Participation/presentations at meetings, conferences, seminars:

-Anderson, P.M., "Deformation and Fracture in Nanolaminated Metallic/Intermetallic Materials, Case Western Reserve University, March 16, 1999.

-Anderson, P.M., Fraser, H.L., Foecke, T., Josell, D., "Deformation and Fracture of Intermetallic Materials," AFOSR Metallic Materials Contractor's Meeting, San Diego, CA, 4-5 March, 1999.

-Xin, X.J., Cheng, Y., and Anderson, P.M., "Dislocation Transmission Through a Bimaterial Interface based on Peierls Dislocation Model, 1998 TMS Fall Meeting, October 12-15, 1998, Rosemont, IL.

-Anderson, P.M., Muju, S., and Mendelsohn, D., Modeling of Microcrack Toughening in Two-Phase Multilayered Media, , 1998 TMS Fall Meeting, October 12-15, 1998, Rosemont, IL.

-Anderson, P.M. and Foecke, T., Slip Propagation in Metallic Multilayered Thin Films, , 1998 TMS Fall Meeting, October 12-15, 1998, Rosemont, IL.

-P.M. Anderson, "Deformation in Nanoscale Layered Metallic Materials," Workshop on properties of ultrafine layered materials, Los Alamos National Labs, April 5, 1998.

-P.M. Anderson and E.R. Kreidler, Jr., "Dislocation-based models of stress-strain behavior in multilayered thin films," MRS Fall '97 Meeting, Boston, MA. Dec. 4, 1997.

-P.M. Anderson, Computer-based Interactive Modules using MathCad," MRS Fall '97 Meeting, Boston, MA. Dec. 4, 1997.

-H.L. Fraser, "Interface Properties and Phase Stabilities in Metallic Multilayers", TMS Fall Meeting, Indianopolis, September 1997.

-H.L. Fraser, "Structural Stabilities in Intermetallic Compounds and Multilayered Materials", Purdue University, October, 1997

-H.L. Fraser, "Structural Stabilities in Multilayered Materials",

Göttingen, October 1997.

-H.L. Fraser, "Ductility, Toughness and Structural Stabilities in Intermetallics and Multilayered Materials", Cambridge University, Cambridge, UK, November 1997

-H.L. Fraser, "Processing and Properties of Advanced Nb-based Intermetallics", PFAMVI, Singapore, November 1997.

-H.L. Fraser, "Strengthening and Toughening Issues in Nb-Ti Based Intermetallics", TMS Annual Meeting, San Antonio, February, 1998.

-H.L. Fraser, "The Interchange between Experimental and Computational Efforts in the Accelerated Maturation of Materials", Mardi Gras Conference, Baton Rouge, LA, February 1998.

-H.L. Fraser, "Microstructure and Mechanical Behavior of Nb Aluminides", 3rd. International Workshop on Ordered Intermetallic Alloys and Composites, HangZhou, PRC, April 1998.

-H.L. Fraser, "Ordering, Deformation Mechanisms, and Oxidation of B2 Nb-based Aluminides", Kyoto Workshop on High-Temperature Intermetallics, Kyoto, Japan, May 1998.

-H.L. Fraser, "Understanding Alloying Addirions to TiAl", Workshop on TiAl, COST 513, Neuchâtel, Switzerland, June 1998.

-H.L. Fraser, "Co-Continuous Ceramic Composites", Robert Bosch Company, Stuttgart, Germany, July 1998.

b. <u>Consultative and advisory functions to other labs and agencies:</u>

-Dr. Fraser has served on the Materials and Structures Panel of the USAF Scientific Advisory Board, involving reviewing of the Materials and Structures programs of AFOSR and Materials Directorate of Wright Facility, Materials Directorate (WL/ML). He has also consulted for the Characterization Facility, Materials Directorate (WL/ML).Dr. Anderson has continued to serve as a reviewer of proposals for DOD and NSF Agencies and interacts on multilayered systems with Dr. P. Hazzledine at UES, Inc., and Drs. Tim Foecke Dan Josell at NIST.

8. New discoveries, inventions, or patent disclosures during grant period

None

9. Honors/Awards during grant period

Anderson, P.M., Recipient, The Boyer Award for Excellence in Teaching Innovation, Ohio State University College of Engineering, May, 1997.